ORNL/TM--9704

DE86 004645

ORNL/TM-9704
Dist. Category UC-20 f,g

Fusion Energy Division

A COMPARATIVE MEASUREMENT OF THE NEUTRAL DENSITY AND PARTICLE CONFINEMENT TIME IN EBT

John C. Glowienka and Roger K. Richards

Date Published - November 1985

Prepared by the
OAK RIDGE NATIONAL LABORATORY
Oak Ridge, Tennessee 37831
operated by
MARTIN MARIETTA ENERGY SYSTEMS, INC.
for the
U.S. DEPARTMENT OF ENERGY
under Contract No. DE-AC05-84OR21400

CONTENTS

Abstract

The neutral density and particle confinement time in the ELMO Bumpy Torus-Scale Experiment (EBT-S) have been determined by two different techniques. These involve a spectroscopic measurement of molecular and atomic hydrogen emissions and a time-decay measurement of a fast-ion population using a diagnostic neutral beam. The results from both diagnostics exhibit identical trends for either estimate, although the absolute values differ by a factor of 2 to 3. The observed variations with fill gas pressure and microwave power from either technique are consistent with measurements of electron density and temperature. In this paper, the measurement techniques are discussed, and the results are compared in the context of consistency with independently observed plasma behavior.

1. Introduction

Particle confinement times are estimated for the EBT plasma by measurements from two different techniques: spectroscopy of atomic and molecular hydrogen emissions, and time decay by charge exchange of an injected fast-ion population. The two techniques provide estimates of EBT particle lifetime τ_p that have the same systematics with external changes (microwave power and fill gas pressure), but that have magnitudes that differ by a factor of between 2 and 3. In addition, the variations of the particle lifetime and neutral density with fill gas pressure and microwave power are consistent with observed variations of electron density and electron temperature.

Section 2 presents a model which relates the measurable quantities to τ_p. Section 3 describes the diagnostic techniques. Section 4 presents the results, and section 5 discusses the results.

2. The Model

The particle confinement time is derived from the particle balance relation,

$$\frac{dn_e}{dt} = \sum_j n_e n_j \langle \sigma v \rangle_j - n_e/\tau_p \ , \tag{1}$$

where n_e is the electron density, n_j is the neutral density for atomic and molecular hydrogen, $\langle \sigma v \rangle_j$ is the ionization rate parameter for the corresponding neutral species, and τ_p is the particle lifetime. Recombination has been neglected because the electron temperature is sufficiently high. Ionization of impurities is not included as an electron source because of their very low densities (Lazar *et al.* 1979). For a steady-state plasma, equation (1) reduces to

$$\tau_p = \left[\sum_j n_j \langle \sigma v \rangle_j \right]^{-1} \ , \tag{2}$$

allowing the determination of the particle lifetime by a measurement of the neutral density. Equation (2) is a local relation and yields a τ_p estimate dependent on the spatial localization of the diagnostic measuring the neutral density. The spatial averaging of the individual diagnostic is presented in section 3, and its influence on results is discussed in section 5.

3. The Measurement Techniques

3.1 *Spectroscopy*

The spectroscopic determination of the neutral density is made with an absolute measurement of photon emissions from the plasma. Since electron collisions on the background neutrals produce photon fluxes proportional to the neutral density, a measurement of this flux along with measurements of the electron density and electron temperature can be combined to estimate the neutral density. In the EBT, the neutral population is composed of both atomic and molecular hydrogen. These can be measured separately because they have different characteristic photon emission spectra.

The H_α (656-nm) line intensity was measured to determine the atomic hydrogen density. The column brightness, B, of this line can be approximated for a monochromator viewing an optically thin plasma in a narrow pencil beam along a minor diameter as

$$B = \frac{2}{4\pi} \int_0^a SRn_H(r)n_e(r)\, dr \tag{3}$$

in units of photons per unit time per unit area per unit solid angle. S is the local electron impact excitation rate coefficient, R is a branching ratio yield for the H_α line, n_H is the local atomic hydrogen density, and n_e is the local electron density. S is a function of both the electron density and the electron temperature. The values for S were taken from Johnson and Hinnov (1973) using the electron temperature measurements from Thomson

scattering, and the electron density was taken to be 1×10^{12} cm^{-3}; in this density range, the excitation rate coefficient is only weakly sensitive to large changes in the electron density. Since the electron temperature is known to be fairly uniform in radius in the core plasma, S will be a constant, and equation (3) can be rewritten to represent a line-averaged atomic neutral hydrogen density, $\bar{n}_H$, as

$$\bar{n}_H = \frac{4\pi B}{SR2\int_0^a n_e d\ell} \quad . \tag{4}$$

The measurement of the atomic neutral density then becomes a measurement of the absolute brightness of the H_α line and the line integral of the electron density, the latter coming from a microwave interferometer.

The brightness of the H_α emission was measured using the optical system shown in figure 1. The photomultiplier, monochromator, window, and mirror were absolutely calibrated as a unit against a standard tungsten lamp. This allowed a conversion of the measured current from the photomultiplier to a brightness from the plasma. With the narrow

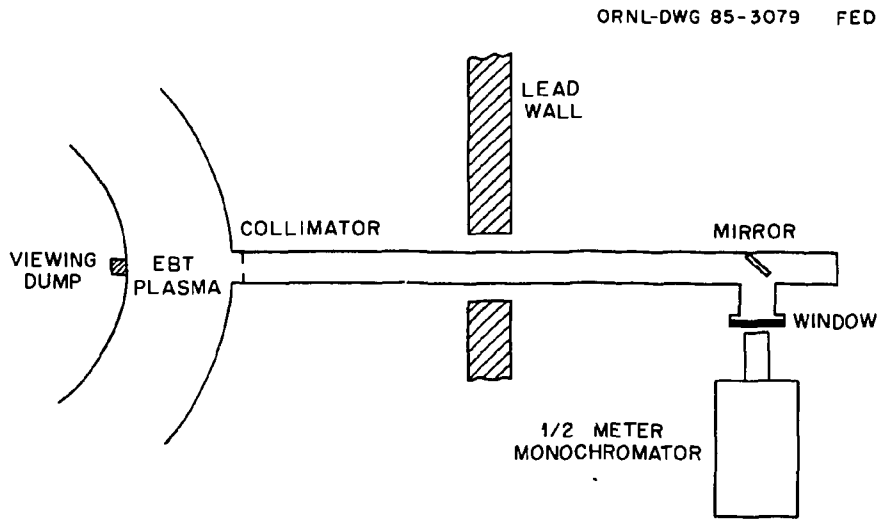

Fig. 1. Schematic of the optical system used in measuring both atomic and molecular emissions.

field of view, the sampling area for viewing the plasma remained nearly constant with a 2.5-cm diameter. The spectral width of the monochromator was set at 1 nm in order to cover the complete H_α line, which had a line width of less than one-tenth of this.

The molecular hydrogen density was determined in a manner similar to that used in measuring the atomic hydrogen. The measurements were made with the same optical system shown in figure 1 with the monochromator tuned to the molecular emission at 490 nm. With the 1-nm resolution used for these measurements, the spectral emission appeared as a continuum; at higher resolution, the individual molecular lines could be found (Gale, Monk, and Lee 1928). The cross section for this emission was taken from Karolis and Harting (1978), and the electron temperature dependence of the rate coefficient was assumed to follow that of the H_α line, since the threshold for excitation for both cross sections is nearly the same and less than the electron temperature under consideration. Using this new excitation rate in the same relation as equation (4) gives the line-averaged molecular density. The sum of the atomic and molecular densities gives the total line-averaged neutral density.

3.2 *Fast-ion decay*

In low-density plasmas ($n \sim 10^{12}$ cm^{-3}), a major ion energy loss process exists from charge exchange on a relatively high background neutral density ($n_0 \sim 10^{10}$ cm^{-3}). This loss mechanism can be exploited for diagnostic purposes by creating a fast-ion population through neutral beam injection, turning off the source of fast ions, and observing the time decay of the fast species with an energy-sensitive detector. If charge exchange is the dominant loss mechanism, the neutral density can be estimated from the decay time τ_D and the charge-exchange rate coefficient $\langle \sigma v \rangle_{cx}$,

$$n_0 = (\tau_D \langle \sigma v \rangle_{cx})^{-1} \ .$$

From equation (2), τ_p is obtained as

$$\tau_p = \tau_D \frac{\langle \sigma v \rangle_{cx}}{\langle \sigma v \rangle_i} .$$

In EBT, the injection is done with a 20-keV, hydrogen diagnostic neutral beam, injecting normal to the B field in a cavity midplane as shown in figure 2. The source produces 20-, 10-, and 6.7-keV neutrals simultaneously. Fast ions are formed all along the neutral beam path through the plasma. In EBT, the electron line density is low ($n_e \ell \sim 10^{13}$ cm^{-2}) so that beam attenuation is a few percent, at most. At formation, the fast ions are trapped and move poloidally in the cavity midplane by cyclotron and ∇B drifts, filling a disk-like volume centered approximately on the toroidal axis. The Larmor and poloidal orbit periods for 10- and 20-keV ions are much shorter than any observed decay time by at

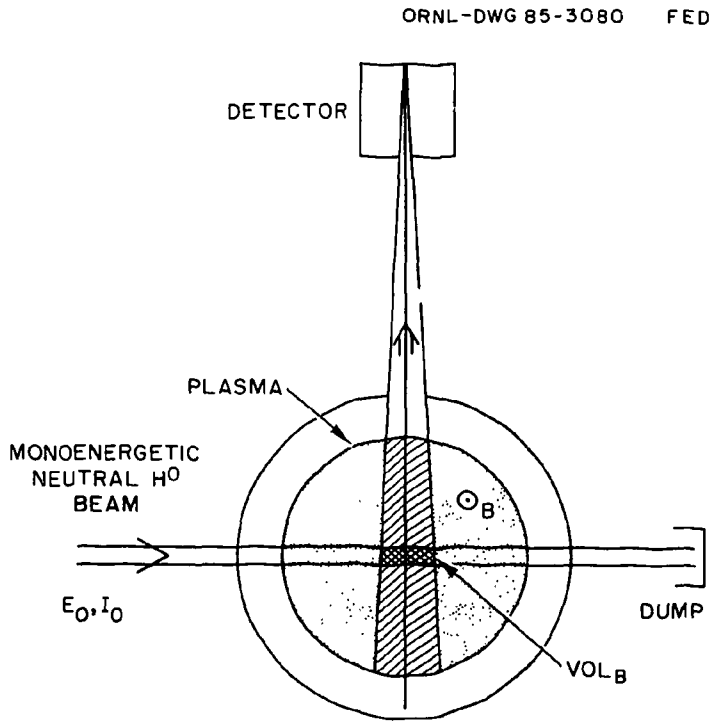

Fig. 2. Geometry of the fast-ion-decay method of determining the neutral density.

least a factor of 10 so that, azimuthally at any radius, the fast-ion density is uniform. The detector, either a small-aperture ($\Omega/4\pi \sim 10^{-7}$), conventional, nitrogen-stripping-cell, electrostatic, charge-exchange energy analyzer (CEX) or a large-aperture ($\Omega/4\pi \sim 10^{-3}$), secondary emission detector (SED), looks along a diameter of the fast-ion disk. A simple model of the radial, fast-ion density profile indicates and measurements verify, as shown in figure 3, that the density of fast ions in the disk varies approximately as $1/r$, where r is the radial distance from the magnetic axis. Consequently, the measurements of τ_p or n_0 are naturally weighted toward the center of the core plasma rather than uniformly weighted over the entire plasma out to the wall.

The CEX detector is sensitive to particles in the range from about 50 eV to about 22 keV and has a 5% energy resolution. The SED has a 100-nm aluminum foil filter to prevent ultraviolet light from striking the cathode and creating a large background signal; the system is sensitive to all particles with energies greater than about 10 keV. Since the plasma ions have a very low average velocity (the plasma ions are cold, $T_i \sim 10$ eV) compared with the beam velocity, the reaction rate is simply the product of the cross section (at the beam energy) and the beam velocity. The charge-exchange reaction rate σv for atomic and molecular neutrals is approximately the same for 10-keV and 20-keV particles, as shown below.

Energy (keV)	Molecular ($cm^3\,s^{-1}$)	Atomic ($cm^3\,s^{-1}$)
10	1.18×10^{-7}	1.15×10^{-7}
20	1.17×10^{-7}	1.16×10^{-7}

The uncertainty is approximately $\pm 25\%$, with most of the uncertainty coming from the cross section ($\pm 20\%$). Within this error bar, this diagnostic is sensitive to the total neutral density rather than to atomic or molecular neutral density. For this work, the reaction rate used with the fast-ion-decay method is

$$\sigma v = 1.2 \times 10^{-7}\,cm^{-3}\,s^{-1} \pm 25\% \ .$$

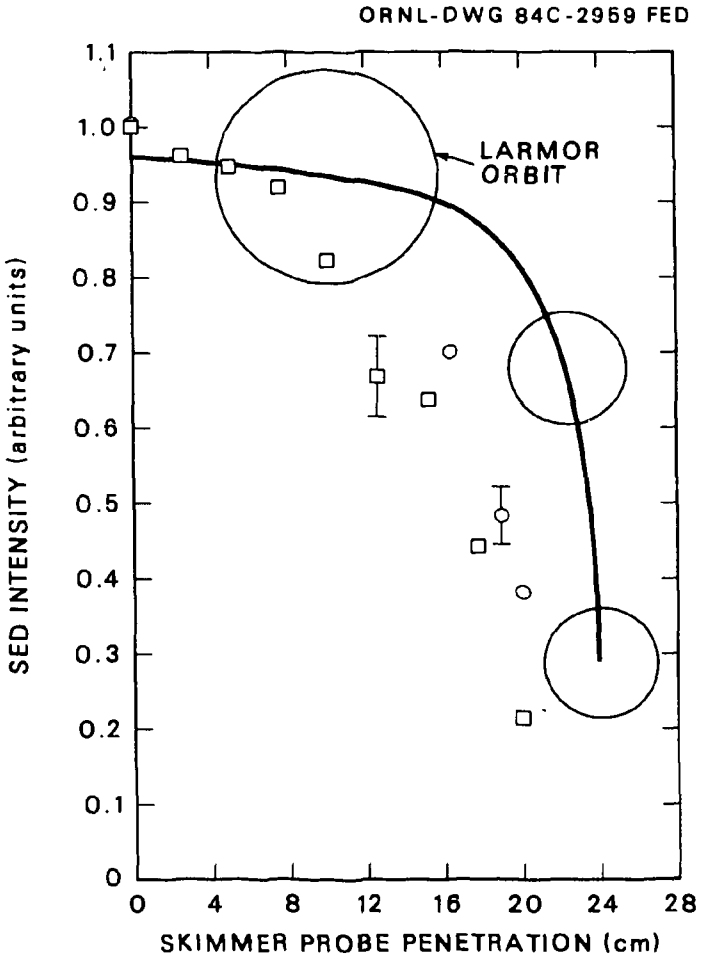

Fig. 3. Solid line: calculated radial profile of the fast-ion density; squares: measured radial profile of the fast-ion density; circles: calculated size of a 20-keV Larmor orbit as a function of radius (hydrogen beam).

4. Results

The data were taken in EBT-S using 28-GHz microwave power (electron cyclotron heating, ECH) at power levels of 50, 100, and 150 kW steady state. The experiment was done at fill gas pressures that placed the operating regime into deep C-mode down through the T-M transition (Colchin *et al.* 1983). A plot of electron temperature from Thomson scattering (Cobble 1985) over this pressure range using 100 kW of ECH is shown in figure 4. Figure 5 shows the estimates of particle lifetime from both diagnostics for the ECH powers as a function of absolute fill gas pressure. Spectroscopic data were taken during a continuous pressure scan; the fast-particle-decay data were taken at discrete pressure points. Figure 6 shows the estimates of total neutral density (atomic and molecular hydrogen) for the conditions given in figure 5.

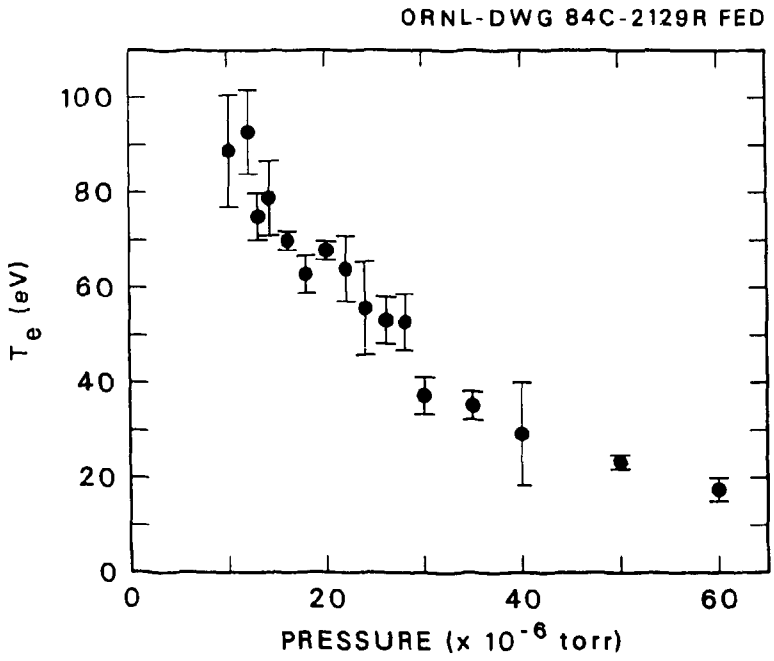

Fig. 4. The variation of the electron temperature with fill gas pressure at 100 kW of electron cyclotron heating (ECH) power. These data were obtained by Thomson scattering (Cobble 1985).

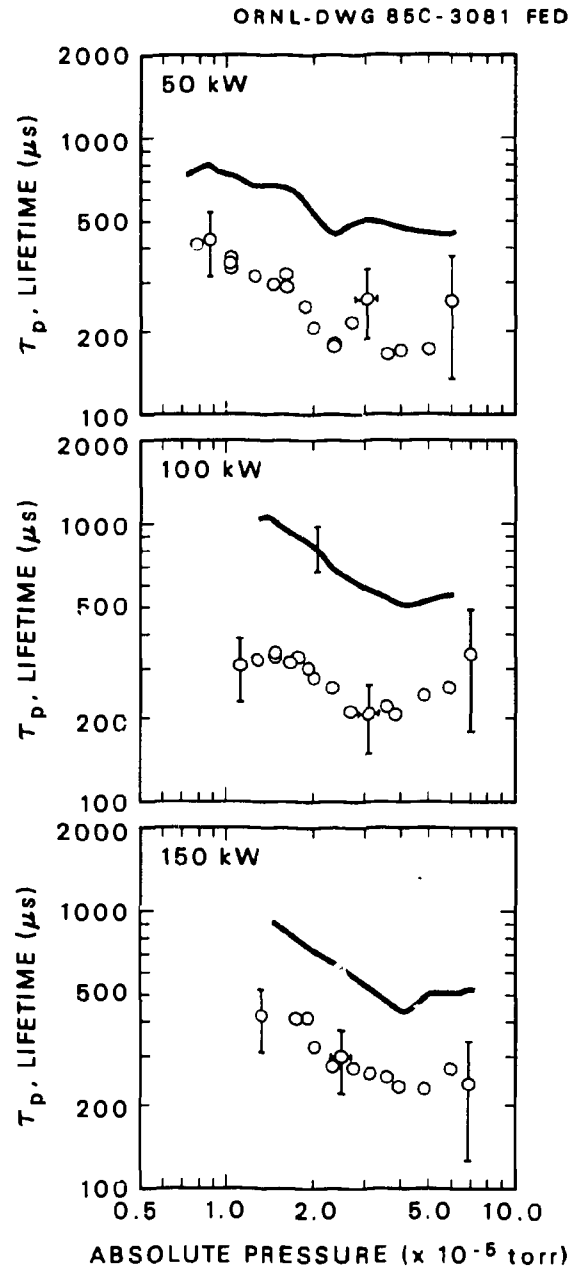

Fig. 5. The variation of the particle confinement time, τ_p, determined by the two diagnostic techniques, as a function of fill gas pressure and at three input microwave powers: 50, 100, and 150 kW. The solid curve is from spectroscopy, and the circles are from fast-ion-decay measurements.

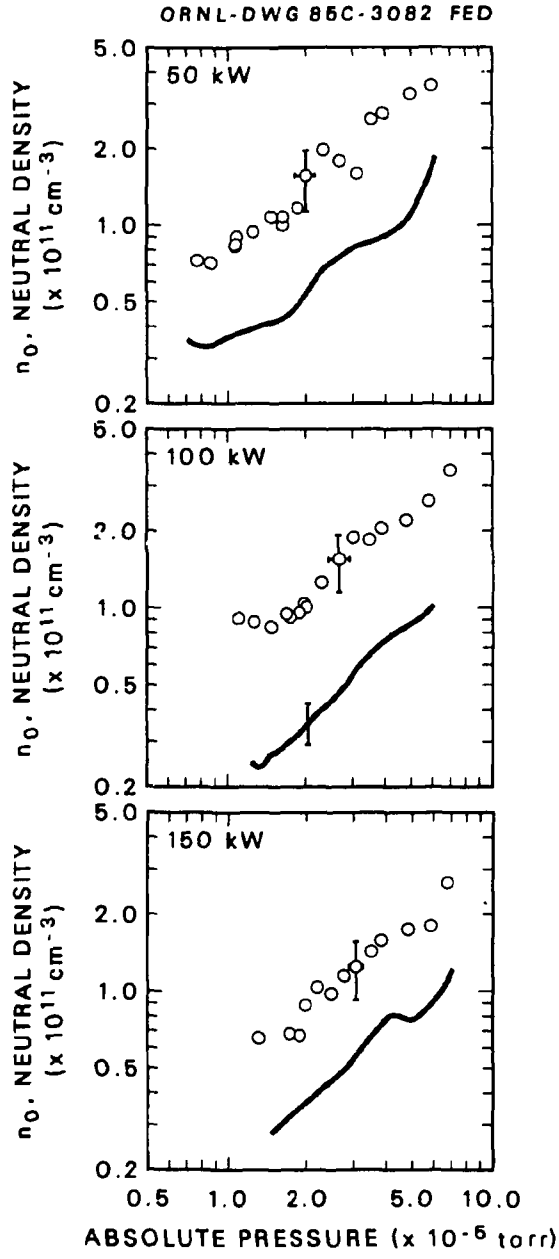

Fig. 6. The values of the neutral density for the conditions of figure 5.

5. Discussion

A comparison of estimates of τ_p or n_0 by the two techniques requires several levels of checks. The most obvious checks are made by comparing the absolute values and by an understanding of the error bars. Equally important checks are the trends of the estimates as plasma conditions are changed and the consistency of the estimates with other plasma measurements.

It is clear from figures 5 and 6 that the large-scale and fine-scale systematics agree very well. For example, the estimates of particle confinement time for both diagnostics exhibit a strong dependence on fill gas pressure but only a weak dependence on ECH power. This provides confidence that the same parameter in each technique is being followed.

The different absolute values cannot be accounted for in the errors; they do not overlap. The uncertainties for both techniques come primarily from the rate coefficients and profile effects. The fast-ion decay is sensitive primarily to neutrals in the core plasma, although there is Larmor radius averaging over several centimeters as indicated by the size of the circles shown in figure 3. However, a model calculation of the line-integrated decay measurement that includes assumed profiles of atomic and molecular neutrals, ions, and electrons indicates that contributions from the surface, where neutral densities are higher than they are in the core, have only a 10% effect, not factors of 2.

The known random uncertainties in the decay method estimate of τ_p are in the charge-exchange rate coefficients ($\pm 25\%$) and the ionization coefficient ($\pm 5\%$ to $\pm 40\%$), depending upon plasma parameters. A possible systematic error could be small-angle collisions that move fast ions out of the field of view, making the decay time appear smaller. However, using classical collisional processes in a Fokker-Planck model with EBT-S parameters obtained in the experiment failed to find systematic effects larger than 10% for the CEX (small field-of-view detector) and failed to find any effect for the SED (large field-of-view detector). Arbitrarily large values of the small-angle collision parameter (three orders of magnitude above that indicated by EBT-S experimental values) produce a

systematic error of 30% for the SED. This would mean a 40% longer decay time. The error bars of the fast-ion-decay method still would not overlap with those of the spectroscopic method.

A critical element of the fast-ion decay is adiabatic orbit behavior of the energetic ions. Calculations that follow orbit trajectories have found that adiabaticity problems occurred for ions with pitch angles an order of magnitude outside the field of view of the SED. A useful experimental check of the entire system, including the effect of adiabaticity, can be made by predicting the molecular hydrogen gas density n_{H_2} in a no-plasma experiment and by comparing the prediction with that provided by an absolutely calibrated ion gage. This test is done with magnetic fields on, without ECH, and by varying the magnitude of the gas fill pressure. As shown in figure 7, the close one-to-one correspondence demonstrates the efficacy of the fast-ion-decay technique.

Errors entering into the spectroscopic determination of neutral density and confinement time included uncertainties in the electron density, the excitation and ionization cross sections, the optical systems efficiency calibration, the viewing solid angle, and the slit area. Of these, the uncertainties in the cross sections were the largest, $\pm 20\%$.

The line-averaged molecular hydrogen density formed approximately one-third of the total neutral density, and this fraction remained constant over the conditions studied in this experiment. A spatial examination of the molecular hydrogen volume emission rate showed flat profiles for the low-power case (50 kW) and slightly hollow profiles at high powers (150 kW), with about one *e*-fold from the outside to the center, at most. The spatial profile for atomic hydrogen had a volume emission rate that peaked in the center under all conditions. This would be expected for the low density (10^{12} cm^{-3}) and small-scale length (10 cm) of this plasma.

The observed variations of τ_p with fill gas pressure and microwave power can be expected from the electron density and temperature in EBT-S. For $n_e \ell \approx 1\text{–}3 \times 10^{13}$ cm^{-2} (obtained at high ECH power in T-mode), the molecular neutrals are strongly attenuated, but the atomic Franck-Condon neutrals are only weakly attenuated. Under these conditions, the center is fueled by ionization of atomic hydrogen, and the surface is

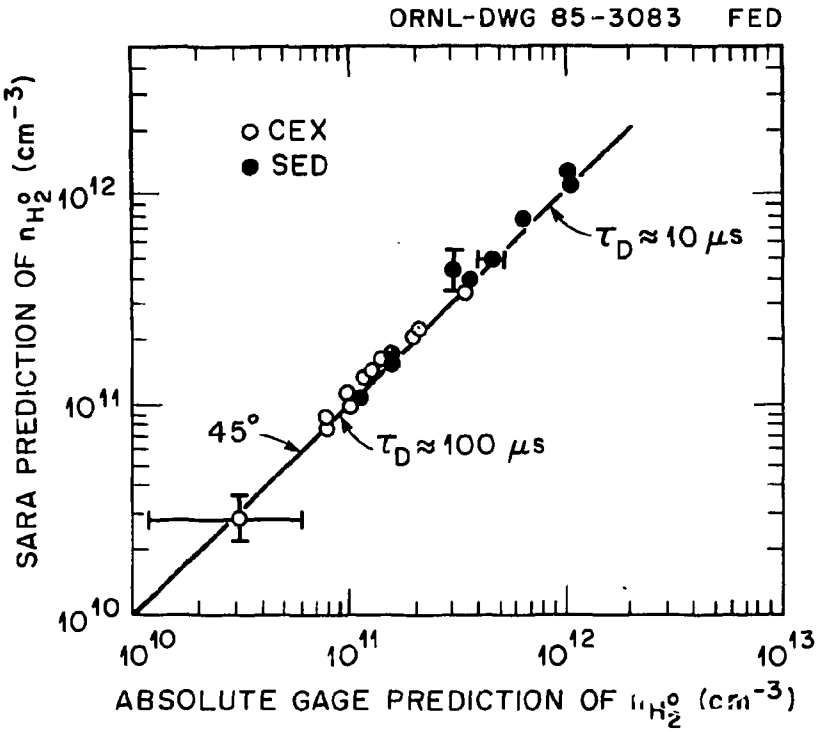

Fig. 7. Results of an experimental check of the fast-ion-decay technique based on a comparison of predictions of molecular hydrogen gas density (n_{H_2}) by the fast-ion-decay technique and by an absolutely calibrated ion gage. This test used the standard EBT-S magnetic field (0.725 T at the cavity midplane on axis), no ECH (no plasma), and various fill pressures as monitored by the calibrated ion gage co-located with the fast-ion-decay diagnostic. The close one-to-one correspondence between the two methods demonstrates the efficacy of the technique.

fueled by both atomic and molecular hydrogen. The core neutral density will vary roughly with the fill gas pressure as seen in figure 6, and the core particle confinement time will vary as the inverse of the fill gas pressure as seen in figure 5. At very high fill gas pressures or low ECH power in C-mode, the electron temperature decreases to where the ionization rate of the neutrals is reduced, and the particle confinement time can increase with

increasing fill gas pressure as seen in figure 5, in particular. Both the center and the surface are fueled principally by atomic hydrogen under these conditions. Since the two diagnostic techniques do not have the same spatial averaging, this will lead to a systematic divergence of the calculated confinement or neutral density because of the spatial changes in the molecular hydrogen profile. However, since the average molecular hydrogen density remains less than the atomic, the difference between high power and low power will be only around 10% and therefore unmeasurable with these techniques.

The variation of the particle confinement time with microwave power can be understood by the dependence of the electron density on microwave power. In EBT, the electron density increases slowly with ECH power, and, since the neutrals are only slightly more attenuated with the slightly higher electron density, the particle confinement time can be expected to show only a weak increase with increasing power.

6. Conclusion

The techniques discussed herein provide estimates that have the same systematics and that provide consistent external checks. The fast-ion-decay method is more direct and simpler than the spectroscopic method. For the determination of the neutral density, only one measurement is required. A third technique, laser fluorescence, may be able to provide another check to determine the absolute magnitude with smaller error bars.

7. Acknowledgments

We are grateful to J. B.Wilgen, W. A. Davis, R. J. Colchin, and J. A. Cobble for contributions of their experimental results and several of their helpful discussions.

ORNL/TM-9704
Dist. Category UC-20 f,g

INTERNAL DISTRIBUTION

1. F. W. Baity
2. D. B. Batchelor
3. L. A. Berry
4. T. S. Bigelow
5. R. J. Colchin
6. R. A. Dory
7. W. A. Davis
8. J. L. Dunlap
9–13. J. C. Glowienka
14. G. R. Haste
15. C. L. Hedrick
16. D. L. Hillis
17. S. Hiroe
18. E. A. Lazarus
19. G. H. Neilson
20. L. W. Owen
21. D. A. Rasmussen
22–26. R. K. Richards
27. M. J. Saltmarsh
28. D. W. Swain
29. C. E. Thomas
30. N. A. Uckan
31. T. Uckan
32. T. L. White
33. J. B. Wilgen
34. J. Sheffield
35–36. Laboratory Records Department
37. Laboratory Records, ORNL-RC
38. Document Reference Section
39. Central Research Library
40. Fusion Energy Division Library
41. Fusion Energy Division Publications Office
42. ORNL Patent Office

EXTERNAL DISTRIBUTION

43. Office of the Assistant Manager for Energy Research and Development, Department of Energy, Oak Ridge Operations, Box E, Oak Ridge, TN 37831
44. J. D. Callen, Department of Nuclear Engineering, University of Wisconsin, Madison, WI 53706
45. R. W. Conn, Department of Chemical, Nuclear, and Thermal Engineering, University of California, Los Angeles, CA 90024
46. S. O. Dean, Director, Fusion Energy Development, Science Applications International Corporation, Gaithersburg, MD 20879
47. H. K. Forsen, Bechtel Group, Inc., Research Engineering, P.O. Box 3965, San Francisco, CA 94205
48. J. R. Gilleland, GA Technologies, Inc., Fusion and Advanced Technology, P.O. Box 85608, San Diego, CA 92138
49. R. W. Gould, Department of Applied Physics, California Institute of Technology, Pasadena, CA 91125
50. R. A. Gross, Plasma Research Library, Columbia University, New York, NY 10027
51. D. M. Meade, Princeton Plasma Physics Laboratory, P.O. Box 451, Princeton, NJ 08544
52. W. M. Stacey, Jr., School of Nuclear Engineering and Health Physics, Georgia Institute of Technology, Atlanta, GA 30332
53. D. Steiner, Rensselaer Polytechnic Institute, Department of Nuclear Engineering, Troy, NY 12181
54. R. Varma, Physical Research Laboratory, Navrangpura, Ahmedabad 380009, India
55. Bibliothek, Max-Planck-Institut fur Plasmaphysik, D-8046 Garching, Federal Republic of Germany

56. Bibliothek, Institut fur Plasmaphysik, KFA, Postfach 1913, D-5170 Julich, Federal Republic of Germany
57. Library, Centre de Recherches en Physique des Plasmas, 21 Avenue des Bains, 1007 Lausanne, Switzerland
58. Bibliotheque, Service du Confinement des Plasmas, CEA, B.P. No. 6, 92 Fontenay-aux-Roses (Seine), France
59. Documentation S.I.G.N., Department de la Physique du Plasma et de la Fusion Controlee, Association EURATOM-CEA, Centre d'Etudes Nucleaires, B.P. 85, Centre du Tri, 38041 Cedex, Grenoble, France
60. Library, Culham Laboratory, UKAEA, Abingdon, Oxfordshire, OX14 3DB, England
61. Library, FOM Instituut voor Plasma-Fysica, Rijnhuizen, Edisonbaan 14, 3439 MN Nieuwegein, The Netherlands
62. Library, Institute for Plasma Physics, Nagoya University, Nagoya 464, Japan
63. Library, International Centre for Theoretical Physics, Trieste, Italy
64. Library, Laboratorio Gas Ionizzati, CP 56, I-00044 Frascati, Italy
65. Library, Plasma Physics Laboratory, Kyoto University, Gokasho Uji, Kyoto, Japan
66. Plasma Research Laboratory, Australian National Laboratory, P.O. Box 4, Canberra, A.C.T. 2000, Australia
67. Thermonuclear Library, Japan Atomic Energy Research Institute Tokai-mura, Ibaraki Prefecture, Japan
68. R. A. Blanken, Office of Fusion Energy, Office of Energy Research, ER-55, Germantown, U.S. Department of Energy, Washington, DC 20545
69. K. Bol, Princeton Plasma Physics Laboratory, P.O. Box 451, Princeton, NJ 08544
70. R. A. E. Bolton, IREQ Hydro-Quebec Research Institute, 1800 Montee Ste.-Julie, Varennes, P.Q. JOL 2P0, Canada
71. R. L. Freeman, GA Technologies, Inc., P.O. Box 81608, San Diego, CA 92138
72. K. W. Gentle, RLM 11.222, Institute for Fusion Studies, University of Texas, Austin, TX 78712
73. R. J. Goldston, Princeton Plasma Physics Laboratory, P.O. Box 451, Princeton, NJ 08544
74. J. C. Hosea, Princeton Plasma Physics Laboratory, P.O. Box 451, Princeton, NJ 08544
75. S. W. Luke, Office of Fusion Energy, Office of Energy Research, ER-55, Germantown, U.S. Department of Energy, Washington, DC 20545
76. E. Oktay, Office of Fusion Energy, Office of Energy Research, ER-55, Germantown, U.S. Department of Energy, Washington, DC 20545
77. D. Overskei, GA Technologies, Inc., P.O. Box 81608, San Diego, CA 92138
78. R. R. Parker, Plasma Fusion Center, 167 Albany Street, Cambridge, MA 02139
79. W. L. Sadowski, Office of Fusion Energy, Office of Energy Research, ER-55, Germantown, U.S. Department of Energy, Washington, DC 20545
80. J. W. Willis, Office of Fusion Energy, Office of Energy Research, ER-55, Germantown, U.S. Department of Energy, Washington, DC 20545
81. A. P. Navarro, Division de Fusion, Junta de Energia Nuclear, Avenida Complutense 22, Madrid (3), Spain
82. Laboratory for Plasma and Fusion Studies, Department of Nuclear Engineering, Seoul National University, Shinrim-dong, Gwanak-ku, Seoul 151, Korea
83. R. E. Price, Office of Fusion Energy, ER-55, Office of Energy Research, U.S. Department of Energy, GTN, Washington, DC 20545
84. J. F. Clarke, Office of Fusion Energy, ER-50, Office of Energy Research, U.S. Department of Energy, GTN, Washington, DC 20545
85. N. A. Davies, Office of Fusion Energy, ER-51, Office of Energy Research, U.S. Department of Energy, GTN, Washington, DC 20545

86. J. M. Turner, Office of Fusion Energy, ER-52, Office of Energy Research, U.S. Department of Energy, GTN, Washington, DC 20545
87. T. C. Simonen, Lawrence Livermore National Laboratory, P.O. Box 5511, (L-640), Livermore, CA 94550
88. T. K. Fowler, Lawrence Livermore National Laboratory, P.O. Box 5511, (L-640), Livermore, CA 94550
89. D. Baldwin, Lawrence Livermore National Laboratory, P.O. Box 5511, (L-630), Livermore, CA 94550
90. G. A. Eliseev, I. V. Kurchatov Institute of Atomic Energy, P.O. Box 3402, 123182 Moscow, U.S.S.R.
91. V. A. Glukhikh, Scientific-Research Institute of Electro-Physical Apparatus, 188631 Leningrad, U.S.S.R.
92. I. Shpigel, Lebedev Physical Institute, Leninsky Prospect 53, 117924 Moscow, U.S.S.R.
93. D. D. Ryutov, Institute of Nuclear Physics, Siberian Branch of the Academy of Sciences of the U.S.S.R., Sovetskaya St. 5, 630090 Novosibirsk, U.S.S.R.
94. V T. Tolok, Kharkov Physical-Technical Institute, Academical St. 1, 310108 Kharkov, U.S.S.R.
95. Library, Institute of Physics, Academia, Sinica, Geijing, People's Republic of China

96–301. Given distribution as shown in TIC-4500, Magnetic Fusion Energy (Category Distribution UC-20 f,g: Experimental and Theoretical Plasma Physics)

REFERENCES

Cobble, J. A. "Evolution of low-density Thomson scattering on ELMO bumpy torus" 1985 *Rev. Sci. Instrum.* **56**, 1018.

Colchin, R. J., Uckan, T., Baity, F. W Berry, L. A., Bieniosek, F. M., Bighel, L., Davis, W. A., Dullni, E., Eason, H. O., Glowienka, J. C., Hallock, G. A., Hast, G. R., Hillis, D. L., Komori, A., Owens, T. L., Richards, R. K., Solensten, L., White, T. L., & Wilgen, J. B. "Plasma properties in the ELMO bumpy torus" 1983 *Plasma Phys.* **25**, 597.

Gale, H. G., Monk, G. S. & Lee, K. O. "Wave-lengths in the secondary spectrum of hydrogen" 1928 *Astrophys. J.* **67**, 89.

Johnson, L. C. & Hinnov, E. "Ionization, recombination, and population of excited levels in hydrogen plasmas" 1973 *J. Quant. Spectrosc. Radiat. Transfer* **13**, 333.

Karolis, C. & Harting, E. "Electron impact dissociation cross sections in hydrogen and deuterium, leading to Balmer alpha and beta emission" 1978 *J. Phys. B: Atom. Molec. Phys.* **11**, 357.

Lazar, N. H., Carpenter, K. H., Tyson, J. M., Warden, E. S., & Moos, H. W. "Spatial distribution of impurities and H neutrals in ELMO bumpy torus, (EBT)" 1979 *Nucl. Fusion* **19**, 571.